Superconducting monolayer deposited on substrate: Effects of the spin-orbit coupling induced by proximity effects

Andrzej Ptok,[1,2,*] Karen Rodríguez,[3,4,†] and Konrad Jerzy Kapcia[1,5,‡]

[1]*Institute of Nuclear Physics, Polish Academy of Sciences, ulica W. E. Radzikowskiego 152, PL-31342 Kraków, Poland*

[2]*Institute of Physics, Maria Curie-Skłodowska University, Plac M. Skłodowskiej-Curie 1, PL-20031 Lublin, Poland*

[3]*Departamento de Física, Universidad del Valle, A. A. 25360, Cali, Colombia*

[4]*Centre for Bioinformatics and Photonics – CiBioFi, Calle 13 No. 100-00, Edificio 320 No. 1069, Cali, Colombia*

[5]*Institute of Physics, Polish Academy of Sciences, Aleja Lotników 32/46, PL-02668 Warsaw, Poland*

(Received 24 April 2017; published 8 February 2018)

Spin-orbit coupling can lead to exotic states of matter and unexpected behavior of the system properties. In this paper, we investigate the influence of spin-orbit coupling induced by proximity effects on a monolayer of superconductor (with *s-wave* or *d-wave* pairing) placed on an insulating bulk. We show that the critical temperatures T_c of the superconducting states can be tuned by the spin-orbit coupling both in the case of on-site and intersite pairing. Moreover, we discuss a possibility of changing the location of the maximal T_c from the half filling into the underdoped or overdoped regimes.

DOI: 10.1103/PhysRevMaterials.2.024801

I. INTRODUCTION

Proximity effects may occur in a situation when two different metals are brought together [1]. In fact, proximity effects can be treated as a *leakage* of some physical properties or quantities from one material to another. As a consequence, for a material that does not possess particular features, a contact with a source material is sufficient enough to acquire them. For the first time it was observed in a superconductor/normal-metal/superconductor (S/N/S) junction [2]. The proximity effect is also experimentally observed as a supercurrent inside an insulator placed between two superconducting materials [3]—a well-known Josephson effect [4].

In modern physics, the proximity effects play an important role in many aspects of spintronics [5–8], where electron spins are exploited as an additional degree of freedom. In this context, the possibility of manipulation of single spins by, e.g., inversion-symmetry-breaking effects is an important issue. The spin-orbit (SO) coupling [9–11], which mixes two spin directions [12], is an example of such an effect. As a consequence, the spin is no longer a good quantum number. These facts lead to several interesting phenomena, which can be applicable in spintronics devices [13–16], e.g., as data storage [17] or quantum computers [18–20].

Recently, a combination of proximity effects and SO coupling has played an important role in studying different types of junctions or heterostructures. An example of this is the interplay between superconductivity and ferromagnetism (F), which can be experimentally investigated in S/F/S Josephson junctions. This interplay leads to in- and out-of-plane magneto-anisotropies of the Josephson currents [21,22], whose direction is controlled by the strength of the SO coupling [23]. In these heterostructures the interfacial Rashba SO coupling has been proposed as the mechanism from which stems the spin-flip Andreev reflection [24].

Similar behavior can be also helpful in the realization of Majorana *quasi*-particles [25–27] in nano-objects such as quantum wires [28]. Recent experiments describe observation of the Majorana bound states in strongly SO-coupled wires, which acquire superconductivity from proximity effects [29–35]. Similar effects are expected in superconducting layers deposited on topological insulators. In such systems, nontrivial topological states can be induced inside superconducting vortices [36,37]. The SO coupling induced in a superconductor through the proximity of a strongly-SO-coupled topological insulator is also observed.

Motivation. The examples presented above show a crucial role of proximity effects in the properties of the system. Recent experiments revealed an extraordinary increase of the critical temperature of FeSe monolayers grown on the (001) surface of $SrTiO_3$ from 8 K [38] to above 65 K [39–42]. Growth on the (110) surface of $SrTiO_3$ is also possible and gives an increase in the critical temperature up to 31.6 K [43–45]. It should be mentioned that the surface of the $SrTiO_3$ exhibits an effective spin-orbit effect [46]. It is generally agreed that mutual exchange of properties between surface and substrate leads to this unusual phenomena. In this context, it seems interesting to study a possible effects of the *induced* SO coupling in superconducting monolayers, which do not show it initially. In this case, changes of global physical properties of such a layer can lead to some novel and unexpected effects, as we show further in this work.

The qualitative process of the induction of an effective SO coupling by the proximity effect can be explained in the following way. The intrinsic SO coupling existing in the bulk substrate modifies wave functions of electrons located in the bulk. A finite hybridization, arising from the overlapping

*aptok@mmj.pl
†karem.c.rodriguez@correounivalle.edu.co
‡konrad.kapcia@ifj.edu.pl

orbitals of atoms in the substrate and the layer, leads to a modification of the band structure of the electrons belonging to the layer [47]. Effects of this modification of the band structure can be described effectively as a spin-orbit coupling in the layer induced by proximity effects.

The proposed idea of SO coupling induced by proximity effects is realizable experimentally, e.g., in the form of $Bi_2Te_3/Fe_{1+y}Te$ [48], WS_2/graphene [49], or Au/graphene [50] heterostructures, graphene on an antiferromagnetic substrate [51] or ferromagnetic one [52–56], or carbon nanotubes coupled to a superconducting substrate [57]. In these systems the proximity effects are crucial for the occurrence of SO coupling. Some other modifications of the heterostructures can also lead to SO coupling, e.g., a change of the impurity structure. These types of manipulations of the effective SO coupling based on proximity effects is realized in nonmagnetic/ferromagnetic bilayers [58]. However, also other possibilities of *induced* SO coupling are studied. A good example is the generation of SO coupling in hydrogenated graphene [59] or by the presence of impurities in graphene [60].

It should be mentioned that the situations described above are different from those where SO coupling exists in the whole volume of a bulk material. In such groups of systems one can distinguish, e.g., topological insulators [12,61,62] or topological superconductors [63–67]. In the latter case superconductivity exists in the presence of SOC, which effectively leads to the emergence of the *p-wave* gap symmetry from a conventional *s-wave* one [67–72]. Moreover, a coexistence of both phenomena is useful for a manipulation of the properties in different types of junctions [73–75].

In this work we analyze the effects of spin-orbit coupling on the critical temperature of a superconducting layer (with both *s-wave* and *d-wave* effective pairing) placed on the surface of an insulator. We solve the effective model for the layer and determine critical temperatures as functions of SO coupling and chemical potential. It is shown that, for fixed spin-orbit interaction the maximal critical temperature occurs in the system with optimal electron doping away from half filling.

The next parts of this work are organized as follows: In Sec. II, we describe the model and method used, whereas in Sec. III the numerical results are presented. Section IV is devoted to the discussion of derived numerical results. Finally, a summary and final comments are included in Sec. V.

II. MODEL AND METHOD

For theoretical studies of the systems described in the previous section we analyze the following model: The system considered is schematically shown in Fig. 1 (left panel). The superconducting monolayer creates an interface with the substrate with strong spin-orbit coupling (these two materials are denoted by SC and SOC, respectively). Because of the proximity effects between SC and SOC, the SO coupling originating from the SOC material enters the SC layer. We describe this scenario, emphasizing the role of the induced SO coupling, by the effective model illustrated schematically in the right panel of Fig. 1 and described in detail below [Eq. (1)]. In our analyses we do not assume a type of superconductivity occurring in the material from which the monolayer is made. Thus, we consider both on-site U_{ii} and intersite U_{ij} pairing

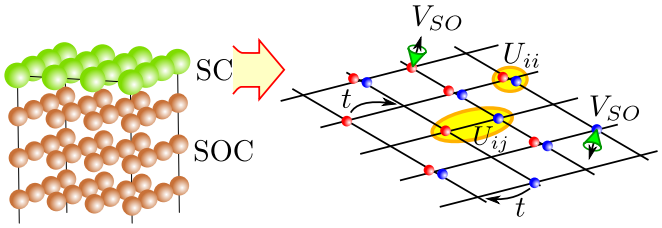

FIG. 1. Schematic representation of the analyzed interface (left) and its effective model (right). We assume the existence of a two-dimensional superconducting (SC) monolayer placed on the surface of an insulator with strong spin-orbit coupling (SOC). We study the superconducting layer with half-spin particles (red and blue balls denote opposite spins), which can move between sites of the lattice (e.g., between the nearest-neighbors with hopping amplitude t). The on-site (U_{ii}) or intersite (U_{ij}) attractive (negative) interactions (schematically indicated by yellow areas) are sources of singlet pairing. An effective spin-orbit-coupling interaction (V_{SO}) in the layer is introduced by proximity effects from the bulk SOC material.

interactions (shown by yellow areas) between two electrons with opposite spin (singlet pairing). This allows us to consider both *s-wave* and *d-wave* superconductors. In the considered model, electrons with both directions of spin (represented by blue and red balls) can move in the superconducting plane between nearest-neighbor (NN) sites with hopping integral t and next-nearest-neighbors (NNN) with hopping amplitude t' (not shown in the schematic picture).

We describe our system by a tight-binding model with the Rashba-type SO interaction [76,77]. The Hamiltonian acquires the form $\hat{H} = \hat{H}_0 + \hat{H}_I + \hat{H}_{\mathrm{SO}}$, where $\hat{H}_0$ denotes the noninteracting term (free electrons), $\hat{H}_I$ denotes the interaction between electron with opposite spins (source of superconductivity in the system), whereas $\hat{H}_{\mathrm{SO}}$ describes the spin-orbit coupling. The terms of the Hamiltonian have the following forms:

$$\begin{aligned}
\hat{H}_0 &= \sum_{ij\alpha}(-t_{ij} - \mu\delta_{ij})\hat{c}^{\dagger}_{i\alpha}\hat{c}_{j\alpha}, \\
\hat{H}_I &= \sum_{ij} U_{ij}\hat{c}^{\dagger}_{i\uparrow}\hat{c}_{i\uparrow}\hat{c}^{\dagger}_{j\downarrow}\hat{c}_{j\downarrow}, \\
\hat{H}_{\mathrm{SO}} &= iV_{\mathrm{SO}}\sum_{i\alpha\beta}\left(\hat{c}^{\dagger}_{i\alpha}\sigma_x^{\alpha\beta}\hat{c}_{i+\hat{y}\beta} - \hat{c}^{\dagger}_{i\alpha}\sigma_y^{\alpha\beta}\hat{c}_{i+\hat{x}\beta} + \mathrm{H.c.}\right),
\end{aligned} \tag{1}$$

where $\hat{c}_{i\alpha}$ ($\hat{c}^{\dagger}_{i\alpha}$) is the annihilation (creation) operator of an electron at the ith site with spin $\alpha \in \{\uparrow,\downarrow\}$, t_{ij} is the hopping integral between the ith and jth sites, μ is the chemical potential, and $U_{ij} < 0$ is the pairing interaction. We consider both, the on-site interaction $U_{ij} = U\delta_{ij}$ corresponding to *s-wave* symmetry of the energy gap, and intersite interaction between nearest neighbors $U_{ij} = U(\delta_{i\pm\hat{x},j} + \delta_{i\pm\hat{y},j})$ corresponding to *d-wave* symmetry of the energy gap [78]. Here, V_{SO} denotes the strength of the effective Rashba SO interaction induced by the proximity effects, while $\sigma_\tau^{\alpha\beta}$ is the $\alpha\beta$ component of the Pauli matrix $\check{\sigma}_\tau$ ($\tau \in \{x,y\}$). Finally, μ is the chemical potential, which determines the filling of the system.

In the momentum space, after employing the broken-symmetry Hartree–Fock mean-field approximation, the

Hamiltonian terms (1) are rewritten in the following forms:

$$\begin{aligned}\hat{H}_0 &= \sum_{k\alpha} \bar{E}_{k\alpha}\hat{c}^{\dagger}_{k\alpha}\hat{c}_{k\alpha},\\ \hat{H}_I &= U\sum_{k}(\Delta_0\gamma(\boldsymbol{k})\hat{c}^{\dagger}_{k\uparrow}\hat{c}^{\dagger}_{-k\downarrow} + \Delta_0^{*}\gamma(\boldsymbol{k})\hat{c}_{-k\downarrow}\hat{c}_{k\uparrow})\\ &\quad - U\sum_{k}|\Delta_0|^2\gamma^2(\boldsymbol{k}),\\ \hat{H}_{\mathrm{SO}} &= \sum_{k\alpha\beta}\left(\check{V}_k\right)_{\alpha\beta}\hat{c}^{\dagger}_{k\alpha}\hat{c}_{k\beta},\end{aligned} \tag{2}$$

where $\bar{E}_{k\alpha} = E_k - \mu$ and $(\check{V}_k)_{\alpha\beta}$ is the $\alpha\beta$ component of $\check{V}_k = 2V_{\mathrm{SO}}[\sin(k_y)\check{\sigma}_x - \sin(k_x)\check{\sigma}_y]$. In the case of a square lattice with hopping between nearest neighbors, $t_{ij} = t(\delta_{i\pm\hat{x},j} + \delta_{i\pm\hat{y},j})$, and next-nearest neighbors, $t_{ij} = t'(\delta_{i\pm(\hat{x}+\hat{y}),j} + \delta_{i\pm(\hat{x}-\hat{y}),j})$, the dispersion relation is given by $E_k = -2t[\cos(k_x) + \cos(k_y)] - 4t'\cos(k_x)\cos(k_y)$. The coefficient $\gamma(\boldsymbol{k})$ describing the symmetry of the order parameter is either 1 or $\cos(k_x) - \cos(k_y)$ for the *s-wave* and *d-wave* symmetry, respectively [78–80]. Finally, $\Delta_0 = 1/N\sum_{\boldsymbol{k}}\langle\hat{c}_{-k\downarrow}\hat{c}_{k\uparrow}\rangle$ is the amplitude of the superconducting order parameter, which is determined variationally by minimizing the grand canonical potential, cf. also Refs. [78,81,82]. Notice that in Hamiltonian (2) we only left terms associated with (extended) BCS-type pairing—the total momentum $\boldsymbol{Q}$ of the Cooper pair is zero: $|\boldsymbol{Q}| = 0$ [80,82–84]. This assumption is valid only if the SO coupling in the monolayer is induced by proximity effects.

A. Absence of superconductivity

When there is no superconductivity in the system, i.e., if $\Delta_0 = 0$ is assumed, from the diagonalization of the Hamiltonian $\hat{H}_0 + \hat{H}_{\mathrm{SO}}$, we retrieve two bands; namely, the upper and lower Rashba bands. The eigenproblem $(\hat{H}_0 + \hat{H}_{\mathrm{SO}})|\Psi_{k,\pm}\rangle = \varepsilon_{k,\pm}|\Psi_{k,\pm}\rangle$ gives the eigenvalues

$$\varepsilon_{k,\pm} = \bar{E}_{k\alpha} \pm 2V_{\mathrm{SO}}\sqrt{\sin^2(k_x) + \sin^2(k_y)} \tag{3}$$

and eigenstates $|\Psi_{k,\alpha}\rangle = \hat{\Psi}^{\dagger}_{k,\alpha}|0\rangle$ $(\alpha = +,-)$, where

$$\begin{pmatrix}\hat{\Psi}^{\dagger}_{k,+}\\ \hat{\Psi}^{\dagger}_{k,-}\end{pmatrix} = \frac{1}{\sqrt{1+\zeta_k^2}}\begin{pmatrix}1 & \zeta_k\\ -\zeta_k & 1\end{pmatrix}\begin{pmatrix}\hat{c}^{\dagger}_{k\uparrow}\\ \hat{c}^{\dagger}_{k\downarrow}\end{pmatrix} \tag{4}$$

and

$$\zeta_k = \frac{(\check{V}_k)_{\uparrow\downarrow}}{\frac{1}{2}(\bar{E}_{k\uparrow} + \bar{E}_{k\downarrow}) + \sqrt{\frac{1}{4}(\bar{E}_{k\uparrow} + \bar{E}_{k\downarrow})^2 + |(\check{V}_k)_{\uparrow\downarrow}|^2}}. \tag{5}$$

We find fourfold-degenerate minimal energy at the nonanalytical points $k_x = \pm k_y$ given by the equation $\sqrt{2}\tan(k_{x(y)})[t + 2t'\cos(k_{x(y)})] = 0$. There are also four saddle points near the energy minimum points, which are located at $\boldsymbol{k} = (0, \pm\mathrm{atan}(V_{\mathrm{SO}}/t))$ and $(\pm\mathrm{atan}(V_{\mathrm{SO}}/t),0)$. The lower and upper Rashba bands correspond to minus "−" and plus "+" signs in the formulas above, respectively, for $V_{\mathrm{SO}} = 2t$ and $t' = 0$ are shown in Fig. 2.

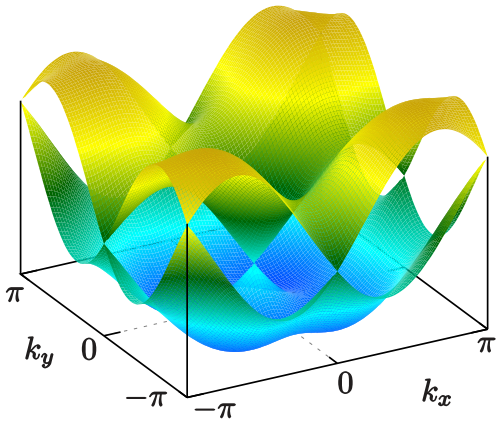

FIG. 2. The lower and upper Rashba bands for $V_{\mathrm{SO}} = 2t$ in the absence of the next-nearest-neighbor hopping ($t' = 0$) and superconductivity ($\Delta_0 = 0$) in the first Brillouin zone for a system on the square lattice.

B. Including superconductivity

Introducing the Nambu spinors $\hat{\Phi}_k = (\hat{c}_{k\uparrow}, \hat{c}_{k\downarrow}, \hat{c}^{\dagger}_{-k\uparrow}, \hat{c}^{\dagger}_{-k\downarrow})^T$, the total Hamiltonian (2) including all terms can be rewritten in the matrix form,

$$\hat{H} = \frac{1}{2}\sum_{k}\hat{\Phi}^{\dagger}_{k}\mathbb{H}_k\hat{\Phi}_k + \frac{1}{2}\sum_{k\sigma}[\bar{E}_{k\sigma} - U|\Delta_0|^2\gamma^2(\boldsymbol{k})], \tag{6}$$

where

$$\mathbb{H}_k = \begin{pmatrix}\bar{E}_{k\uparrow} & (\check{V}_k)_{\uparrow\downarrow} & U\Delta_0\gamma(\boldsymbol{k}) & 0\\ (\check{V}_k)^{*}_{\uparrow\downarrow} & \bar{E}_{k\downarrow} & 0 & U\Delta_0\gamma(\boldsymbol{k})\\ U\Delta_0^{*}\gamma(\boldsymbol{k}) & 0 & -\bar{E}_{-k\uparrow} & -(\check{V}_{-k})_{\downarrow\uparrow}\\ 0 & U\Delta_0^{*}\gamma(\boldsymbol{k}) & -(\check{V}_{-k})^{*}_{\downarrow\uparrow} & -\bar{E}_{-k\downarrow}\end{pmatrix}. \tag{7}$$

In the above expression, $(\check{V}_k)_{\alpha\beta}$ correspond to the matrix elements of the spin-orbit coupling matrix $\check{V}_k$ defined previously. The grand canonical potential of the system is determined by

$$\begin{aligned}\Omega &= -\frac{1}{2}k_BT\sum_{k,n=1}^{4}\ln\left(1 + \exp\left(\frac{-\lambda_{kn}}{k_BT}\right)\right)\\ &\quad + \frac{1}{2}\sum_{k\sigma}[\bar{E}_{k\sigma} - U_0|\Delta_0|^2\gamma^2(\boldsymbol{k})],\end{aligned} \tag{8}$$

where λ_{kn} $(n = 1,\ldots,4)$ are the eigenvalues of the matrix $\mathbb{H}_k$, which is given by Eq. (7), and T is the absolute temperature.

III. NUMERICAL RESULTS

The calculations are carried out for a two-dimensional square lattice of a size $N_X \times N_Y = 200 \times 200$ with the periodic boundary conditions. In the case of the BCS state this size corresponds to the thermodynamic limit [85]. We find the ground state of the system as the global minimum of Ω with respect to Δ_0 for a given set of model parameters $\{\mu, V_{\mathrm{SO}}, T\}$, using the procedure described in Ref. [86]. We take the NN hopping ($|t| = 1$) as the energy unit, while the NNN hopping is set as $t' = -0.1t$. As a consequence, the half filling

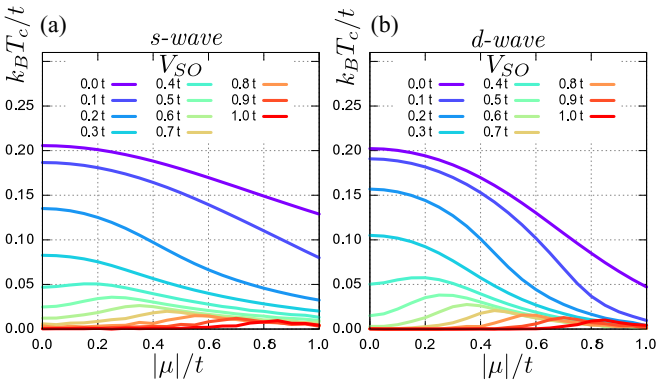

FIG. 3. Critical temperature as a function of the chemical potential μ for several spin-orbit coupling strengths V_{SO} (as labeled) for a square lattice in the absence of the next-nearest-neighbor hopping ($t' = 0$). Two types of superconductivity are considered: (a) *s-wave* and (b) *d-wave*.

(i.e., $n = 1$) is attained for $\mu/t = 0$ and $\mu/t = -0.4$ in the absence and in the presence of the NNN hopping, respectively. Moreover, in all of our calculations presented here, we set the interaction strengths to $U/t = -2$ and $U/t = -1.25$ for *s-wave* and *d-wave* symmetry, respectively. These choices of U interactions give approximately equal critical temperatures T_c at half filling in the absence of the NNN hopping for both symmetries considered. Nevertheless, the choice of specific values of attractive $U < 0$, at least for not very large values of $|U|/t$ [82], should not change qualitatively the results presented further in the paper.

A. Absence of next-nearest-neighbor hopping ($t' = 0$)

We start analyzing the influence of the spin-orbit coupling V_{SO} on the critical temperature T_c as a function of the chemical potential μ in the absence of NNN hopping ($t' = 0$). The electron concentration n (the filling of the system) is a monotonically increasing function of μ. We define T_c as the temperature at which the amplitude of the superconducting order parameter Δ_0 vanishes for a given $\{\mu, V_{SO}\}$. As we will show, $T_c = T_c(\mu, V_{SO})$ is not a trivial monotonic function of μ and V_{SO}. All transitions found in the system are second-order (continuous) ones.

The phase diagrams for a few values of V_{SO} are presented in Fig. 3. For $V_{SO} = 0$, we find monotonic decreasing behavior of T_c as a function of $|\mu|$ with maximum at the half filling (for $\mu = 0$), i.e., $T_c^{\max}(V_{SO} = 0) = T_c(\mu = 0, V_{SO} = 0)$. Switching the SO coupling on, the situation changes and the maximal T_c is located away from the half filling (for $\mu \neq 0$), i.e., $T_c^{\max}(V_{SO} \neq 0) = T_c(\mu \neq 0, V_{SO} \neq 0)$. For fixed $V_{SO} \neq 0$, T_c is a nonmonotonic function of μ with a local minimum at $\mu = 0$. However, for sufficiently small SO values, smaller than $V_{SO} \approx 0.36t$, the behavior changes very slightly and it cannot be seen unambiguously. The continuous increase of T_c as the doping increases leads to a growth of T_c due to the presence of SO coupling. The same qualitative behavior is observed in both symmetry cases, but there are some quantitative differences between them. Particularly, from Fig. 3 it is seen that the superconductivity is more sensitive to the doping for *d-wave* symmetry, i.e., for fixed V_{SO} temperature T_c varies more with

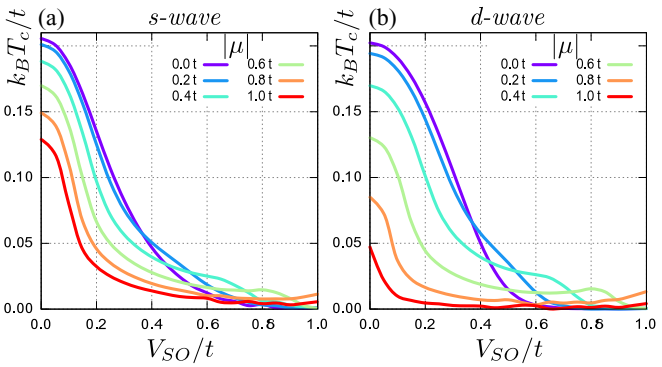

FIG. 4. Critical temperature as a function of spin-orbit coupling V_{SO} for several chemical-potential values μ (as labeled) in the absence of the next-nearest-neighbor hopping ($t' = 0$). Two types of superconductivity are considered: (a) *s-wave* and (b) *d-wave*.

changing μ in the presence of *d-wave* pairing. In contrast, V_{SO} more strongly suppresses *s-wave* superconductivity [i.e., $T_c(\mu = 0, V_{SO})$ at half filling decreases faster with increasing of V_{SO} for the *s-wave* case].

To gain a better understanding of the situation, we plot T_c, but this time as a function of the SO coupling, for several values of the chemical potential, as shown in Fig. 4. It is found that, for fixed μ, T_c is not a monotonically decreasing function of V_{SO} (if the chemical potential or, equivalently, doping is away from half filling). For small values of V_{SO}, an increase of the SO coupling reduces T_c. However, at sufficiently large μ and for larger values of the SO coupling, the temperature T_c increases again. This revival is clearly seen in this *cross section* of the k_BT versus V_{SO} phase diagrams, where the critical temperature for larger $|\mu|$ exceeds the values obtained at lower values of μ, particularly those derived for the half filling.

B. Presence of next-nearest-neighbor hopping ($t' \neq 0$)

Next, we investigate the behavior of the system in the presence of the NNN hopping ($t' = -0.1t$). In such a case

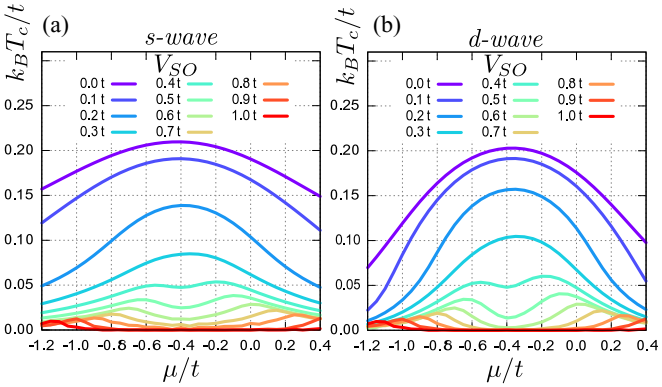

FIG. 5. Critical temperature as a function of the chemical potential μ for several spin-orbit coupling values V_{SO} (as labeled) for a square lattice in the presence of the next-nearest-neighbor hopping term ($t' = -0.1t$). Two types of superconductivity are considered: (a) *s-wave* and (b) *d-wave*. The half filling condition corresponds to $\mu = -0.4t$.

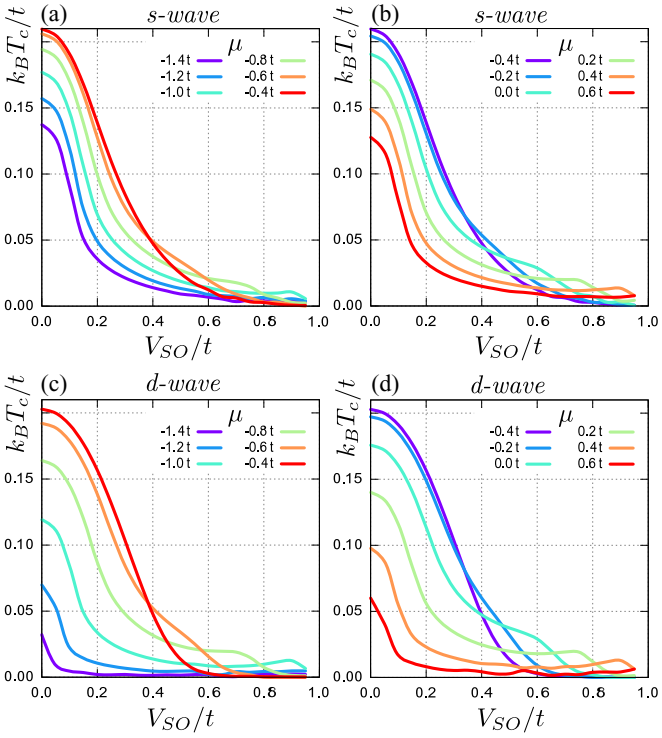

FIG. 6. Critical temperature as a function of spin-orbit coupling $V_{\rm SO}$ for several chemical-potential values μ (as labeled) in the presence of NNN hopping ($t' = -0.1t$). Two types of superconductivity are considered: (a), (b) *s-wave* and (c), (d) *d-wave*. The half filling condition corresponds to $\mu = -0.4t$. Panels (a) and (c) present curves for an underdoped system, whereas panels (b) and (d) are obtained in the overdoped regime.

the dependence of T_c as a function of μ loses its symmetry around half filling; see Figs. 5 and 6. Similarly as before, we observe a substantial influence of the spin-orbit coupling on the μ dependence of T_c, which is stronger in the *d-wave*-symmetry case. Again, we obtain a growth of T_c over its half-filling value as the chemical potential changes away from the half filling for fixed $V_{\rm SO} > 0$ (Fig. 5). However, the value of maximal T_c in the overdoped regime (i.e., $\mu > -0.4t$) is larger than that obtained for underdoped system (i.e., $\mu < -0.4t$). T_c as a function of $V_{\rm SO}$ for fixed μ exhibits similar properties as discussed for $t' = 0$ previously, although the values of T_c for underdoped and overdoped system differ from each other (Fig. 6) As we indicated before, the half-filling condition $n = 1$ for the model parameter used corresponds to $\mu = -0.4t$. One should remember that the value of T_c, for a given $\{\mu, V_{\rm SO}\}$, depends also on t'.

IV. DISCUSSION

We now discuss our results in terms of (i) the density of states of the noninteracting system and (ii) the nontrivial superconductivity induced by the SO coupling. In relation to superconducting state, the density of states of the noninteracting system at the Fermi level affects the critical temperatures and critical magnetic fields. This relation between these macroscopic and microscopic quantities has been described in the

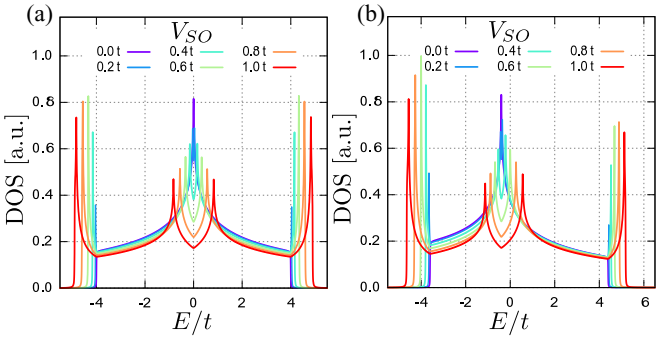

FIG. 7. Noninteracting total density of states for (a) $t' = 0$ and (b) $t' = -0.1t$ and for several values of $V_{\rm SO}$ (as labeled). The Fermi level is located at $E = -4t'$ for the half filling. The shape of the noninteracting density of states is not dependent on μ. Only the Fermi level E_F depends on μ ($E_F = \mu - 4t'$).

pioneering papers of Bardeen, Cooper, and Schrieffer [83,84]. On the other hand, the existence of the SO coupling in the system leads to a mixing of electron states with opposite spins, which is clearly seen in the expressions for the eigenvectors of noninteracting system given by Eq. (4). As a consequence, we can expect a realization of the nontrivial triplet pairing in the system [67–72].

A. Density of states

To understand the behavior of the system described in the previous section, i.e., the dependence of T_c as a function of μ and $V_{\rm SO}$, we calculate the noninteracting partial density of states (DOS) [87]:

$$\rho_{\pm}(E) = \frac{1}{N}\sum_{\boldsymbol{k}} \delta(\varepsilon_{\boldsymbol{k},\pm} - E), \tag{9}$$

where the eigenvalues $\varepsilon_{\boldsymbol{k},\pm}$ of the $\hat{H}_0 + \hat{H}_{\rm SO}$ are given by Eq. (3). In our case the total density of states is given by $\rho(E) = \rho_+(E) + \rho_-(E)$.

In Fig. 7, we present DOS for both cases $t' = 0$ and $t' \neq 0$ for different values of $V_{\rm SO}$. We retrieve symmetric profiles around $E = 0$ in the absence of the NNN term as expected [Fig. 7(a)]. On the contrary, in the presence of the NNN hopping, the symmetry around $E = -4t'$ is lost. This fact reflects the behavior already retrieved in the T-versus-μ phase diagram presented in Figs. 3 and 5. From the results presented in Fig. 7 one can conclude that a nonzero SO coupling $V_{\rm SO}$ leads to (i) a division of the Van Hove (central) peak in $\rho(E)$ at $E = -4t'$, and (ii) the emergence of additional peaks near both band edges. The changes reported in the DOS are the result of the modifications of the band structure due to the SO coupling [Fig. 8(a)]. The double-peak structure of $\rho(E)$ near $E \approx -4t'$ is the result of an existence of energy local minima (maxima) of the dispersion relation near points X and Y of the Brillouin zone in the lower (upper) Rashba band (cf. also Fig. 2 for $t' = 0$). On the contrary, the peaks at the edges are due to the existence of four saddle points in every Rashba band with energies $E_{\rm sad} = \mp 2t\{1 + [1 + (V_{\rm SO}/t)^2]^{1/2}\}$ near the Γ and M points, where the $\mp$ signs correspond to the lower and upper Rashba bands, respectively.

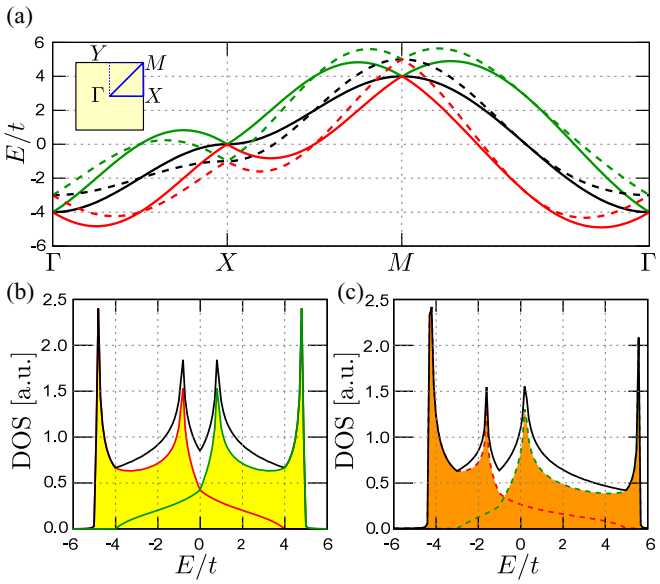

FIG. 8. (a) The band structure along high-symmetry points Γ–X–M–Γ (see left inset for locations of the points) for $t' = 0$ (solid lines) and $t' = -0.25t$ (dashed lines): the electron band structure (for $V_{SO} = 0$) is represented by the black lines, whereas the lower and the upper Rashba bands for $V_{SO} = 1t$ are indicated by red and green lines, respectively. The lower panels show the total [$\rho(E)$, black line] and partial [$\rho_{\mp}(E)$, red and green lines for the lower and the upper Rashba bands] densities of states for (b) $t' = 0$ and (c) $t' = -0.25t$, with spin-orbit coupling $V_{SO} = 1t$.

Assuming that the critical temperature is given by the standard BCS formula, then one gets $T_c \sim \exp[-1/\rho(E_F)]$ [83,84]. It is rather justified for the values of U/t considered in the present work. Using the relation between total and partial DOS, we obtain that $T_c \sim \exp\{-1/[\rho_+(E_F) + \rho_-(E_F)]\}$, where $E_F = \mu - 4t'$ in a case of the square lattice with the NNN hopping considered here. To illustrate this fact, the two partial DOS are presented in Figs. 8(b) and 8(c). A direct comparison with Fig. 7 shows that the greatest influence on the total DOS comes only from one Rashba band. In the case of the underdoped system it is the lower Rashba band, while in the overdoped case the upper Rashba band is the crucial one.

In the results presented in this paper, for T_c as a function of μ and for $V_{SO} \neq 0$, we have not found any consequences of the existence of the additional narrow peaks in the DOS $\rho(E)$ at both edges of the Rashba bands. It can be due to the fact that these peaks are located solely at the Fermi level for very small either electron or hole concentrations in the system (i.e., at $n \approx 0$ or $n \approx 2$, respectively). However, this behavior can have an important role in extremely dilute systems, e.g., in the BCS-BEC crossover region [88–90].

B. Nontrivial pairing

As indicated above, in the presence of SO coupling the electron spin is no longer a good quantum number. Despite the fact that we have labeled the system under consideration to present either *s-wave* or *d-wave* symmetry of the superconducting order parameter, the SO coupling can *effectively introduce* a *p-wave* superconductivity. This possibility is well known and described in the literature; see, e.g., Refs. [67–72]. In this aspect a mutual relation between the pairing in electron and quasiparticle spaces is important (see Appendix). As a consequence of this matter, it is possible to realize the nontrivial *triplet* pairing in the considered system in the presence of the SO coupling, even if conventional pairing (for both initial gap symmetries, i.e., *s-wave* and *d-wave*) is a source of superconductivity.

This issue can be described by a transformation, which changes the basis from the original one into the helicity basis and one can find a ratio [cf. Eq. (A4)] between triplet and singlet pairing (more details can be found in Appendix). This ratio is a nontrivial function of the doping μ, the NNN hopping t', and the SO coupling V_{SO}. We found that this ratio is an increasing function of V_{SO} and doping in the neighborhood of the half filling. It changes from zero (at half-filling and small V_{SO}) to a few tens (at optimal doping, i.e., doping for which T_c is the largest one at fixed V_{SO}). Moreover, it depends on the momentum as consequence of nonisotropic symmetry of the gap in considered system (i.e., for the *d-wave* case).

V. SUMMARY AND FINAL REMARKS

The spin-orbit coupling can lead to different unexpected behaviors in various systems. In this paper, we discuss the influence of spin-orbit coupling on superconducting states in the presence of on-site (*s-wave*) or intersite (*d-wave*) pairing in a monolayer with spin-orbit coupling induced by the proximity effects. In particular, we discuss the temperature versus doping phase diagram in detail. In our work, tuning the doping away from the half filling, we demonstrate that the critical temperature can be a nonmonotonic function of the spin-orbit coupling. Moreover, we have shown that for fixed value of the spin-orbit interaction the maximal value of the critical temperature is obtained for the underdoped or overdoped regimes, i.e., away from half filling. Therefore, our results highlight the effects of the spin-orbit coupling on superconducting properties of the system.

These results may be particularly relevant due to the feasibility of experimental realization of superconducting nano- and spintronic devices where a temperature dependence on the spin-orbit coupling using doped systems can enhance critical temperatures T_c significantly rather than those at half filling. It could be of a great importance due to the fact that for applications of superconducting materials systems with larger T_c are preferred.

The modifications of the T_c by the spin-orbit coupling have also been discussed within the Werthamer–Helfand–Hohenberg (WHH) theory [91], which describes the orbitally limited upper critical field of dirty type-II superconductors. In the WHH theory T_c is found as a function of a parameter describing the system [92], e.g., it can be the SO coupling. Similar to the findings of the present work, the WHH theory predicts that an increase in the spin-orbit coupling can lead to an increase in T_c [93]. Moreover, similar behavior of T_c can be observed in systems with nontrivial *p-wave* pairing [94].

The results presented are described in the context of solid-state physics, e.g., a superconducting monolayer on a surface of

an insulator with strong spin-orbit coupling (e.g., topological insulator). In this system, as a consequence of the proximity effects, the SO is induced in the layer and affects the physical properties of the superconductor. However, the investigations of the effects of the SO coupling on superconductivity beyond the described heterostructure can be performed with ultracold atomic gases on the optical lattices. [95]. The realization of the artificial SO coupling in such systems is possible [69,96–99]. Such experiments are important towards to an experimental realization of atomic superfluids with topological excitations.

ACKNOWLEDGMENTS

The authors are thankful to T. Domański, Sz. Głodzik, A. Kobiałka, P. Piekarz, and K. I. Wysokiński for very fruitful discussions and comments. K.R. acknowledges the support from CIBioFi and the Colombian Science, Technology and Innovation Fundation—COLCIENCIAS "Francisco José de Caldas" under project 1106-712-49884 (Contract No. 264-2016) and—General Royalties System (Fondo CTeI-SGR) under Contract No. BPIN 2013000100007. The support from UMO-2016/20/S/ST3/00274 (A.P.), UMO-2016/21/D/ST3/03385 (K.J.K.) and UMO-2017/24/C/ST3/00276 (K.J.K.) projects by Narodowe Centrum Nauki (NCN, National Science Centre, Poland) is also acknowledged.

APPENDIX: NONTRIVIAL SUPERCONDUCTIVITY INDUCED BY SPIN-ORBIT COUPLING

Formally, in the original basis, the singlet Cooper pairs are described by the Hamiltonian (2). It formally corresponds to a pairing of electrons with opposite spin and momentum. An existence of the SO coupling in the system leads to a mixing of the spins, which is clearly shown by Eq. (4). As a consequence, in the noninteracting system, one can discuss the existence of the lower and upper Rashba bands, which has been described in Sec. II A.

Technically, the Hamiltonian of the system in the presence of superconductivity can be rewritten in a helicity basis of eigenstates (4). Then, the matrix form (7) of the Hamiltonian is formally given as $\hat{H} = \frac{1}{2}\sum_{\boldsymbol{k}} \hat{\varphi}_{\boldsymbol{k}}^{\dagger}\tilde{\mathbb{H}}_{\boldsymbol{k}}\hat{\varphi}_{\boldsymbol{k}} + \text{const.}$, where

$$\tilde{\mathbb{H}}_{\boldsymbol{k}} = \begin{pmatrix} \varepsilon_{\boldsymbol{k},+} & 0 & \tilde{\Delta}_{++}(\boldsymbol{k}) & \tilde{\Delta}_{+-}(\boldsymbol{k}) \\ 0 & \varepsilon_{\boldsymbol{k},-} & \tilde{\Delta}_{-+}(\boldsymbol{k}) & \tilde{\Delta}_{--}(\boldsymbol{k}) \\ \tilde{\Delta}_{++}^{*}(\boldsymbol{k}) & \tilde{\Delta}_{-+}^{*}(\boldsymbol{k}) & -\varepsilon_{-\boldsymbol{k},+} & 0 \\ \tilde{\Delta}_{+-}^{*}(\boldsymbol{k}) & \tilde{\Delta}_{--}^{*}(\boldsymbol{k}) & 0 & -\varepsilon_{-\boldsymbol{k},-} \end{pmatrix}, \tag{A1}$$

$\hat{\varphi}_{\boldsymbol{k}} = (\hat{\Psi}_{\boldsymbol{k},+}, \hat{\Psi}_{\boldsymbol{k},-}, \hat{\Psi}_{-\boldsymbol{k},+}^{\dagger}, \hat{\Psi}_{-\boldsymbol{k},-}^{\dagger})^{T}$, and $\hat{\Psi}_{\boldsymbol{k},\pm}$ are defined by (4); for details cf. Ref. [71]. Similarly as previously, "plus" and "minus" signs correspond to helicity basis (i.e., the Rashba bands). Superconducting order parameters (SOPs) $\tilde{\Delta}_{++}$ and $\tilde{\Delta}_{--}$ describe the intraband pairing, whereas parameters $\tilde{\Delta}_{+-}$ and $\tilde{\Delta}_{-+}$ are associated with the interband pairing (which is schematically shown in Fig. 9). Notice that they are dependent on $\boldsymbol{k}$. The new SOPs in the helicity basis are defined as $\tilde{\Delta}_{\alpha\beta} = \langle\hat{\Psi}_{-\boldsymbol{k},\alpha}^{\dagger}\hat{\Psi}_{\boldsymbol{k},\beta}\rangle$. The first type of pairing ($\alpha = \beta$) corresponds to singlet pairing of electrons in the helicity basis [Fig. 9(b), it contains not only *s-wave* but also *d-wave* and higher angular-momentum contributions], while the second one ($\alpha \neq \beta$) is associated with the triplet pairing in the helicity basis [Fig. 9(c), it contains not only *p-wave* but also *f-wave* and higher angular-momentum contributions].

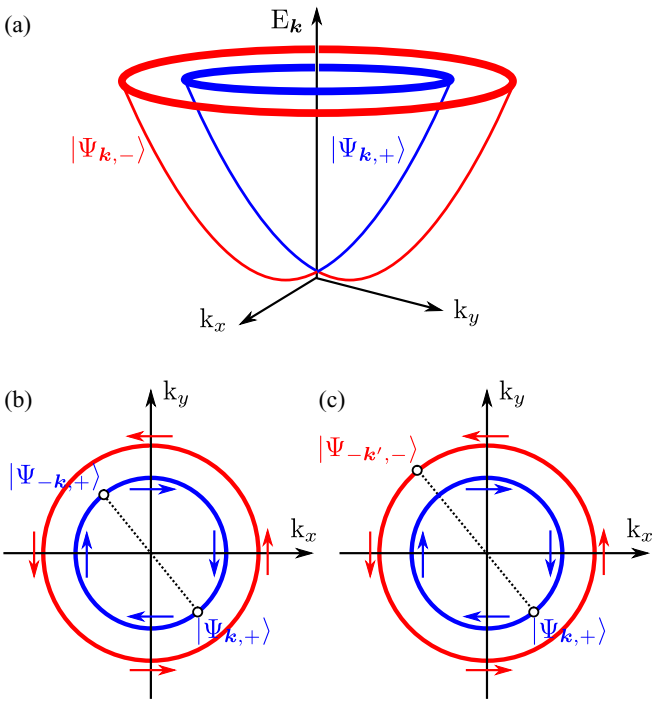

FIG. 9. Schematic illustration of the influence of the SO coupling on the band structure. (a) In the presence of the SO the spin degeneracy is lifted and two Rashba bands $|\Psi_{\boldsymbol{k},\alpha}\rangle$ with different indexes ($\alpha = -,+$) of pseudospin (helical spin texture) arise (the arrows mark the pseudospin directions). The lower $|\Psi_{\boldsymbol{k},-}\rangle$ and upper $|\Psi_{\boldsymbol{k},+}\rangle$ Rashba bands are denoted by red and blue lines, respectively. Examples of the intraband [panel (b)] and interband [panel (c)] pairings are shown.

Using transformation (4), one can express the SOPs in the helicity basis by the SOP in the original basis [81,100]:

$$\begin{aligned}\tilde{\Delta}_{++}(\boldsymbol{k}) &= \tilde{\Delta}_{--}(\boldsymbol{k}) \\ &= U\Delta_0\gamma(\boldsymbol{k})\frac{1+\zeta_{\boldsymbol{k}}\zeta_{-\boldsymbol{k}}}{\sqrt{1+\zeta_{\boldsymbol{k}}^2}\sqrt{1+\zeta_{-\boldsymbol{k}}^2}},\end{aligned} \tag{A2}$$

$$\begin{aligned}\tilde{\Delta}_{+-}(\boldsymbol{k}) &= -\tilde{\Delta}_{+-}(\boldsymbol{k}) \\ &= U\Delta_0\gamma(\boldsymbol{k})\frac{\zeta_{\boldsymbol{k}}-\zeta_{-\boldsymbol{k}}}{\sqrt{1+\zeta_{\boldsymbol{k}}^2}\sqrt{1+\zeta_{-\boldsymbol{k}}^2}},\end{aligned} \tag{A3}$$

where $\zeta_{\boldsymbol{k}}$ is given by Eq. (5) From these relations, the ratio between triplet and singlet component of the nonisotropic gap superconductor depends on momentum and can be expressed as

$$\eta_{\boldsymbol{k}} = \frac{\tilde{\Delta}_{+-}(\boldsymbol{k})}{\tilde{\Delta}_{++}(\boldsymbol{k})} = \frac{\zeta_{\boldsymbol{k}}-\zeta_{-\boldsymbol{k}}}{1+\zeta_{\boldsymbol{k}}\zeta_{-\boldsymbol{k}}}. \tag{A4}$$

Notice also the fact that $|\tilde{\Delta}_{+-}(\boldsymbol{k})|^2 + |\tilde{\Delta}_{++}(\boldsymbol{k})|^2 = |\Delta_0|^2$.

[1] P. G. de Gennes, Boundary effects in superconductors, Rev. Mod. Phys. **36**, 225 (1964).

[2] R. Holm and W. Meissner, Messungen mit Hilfe von flüssigem Helium. XIII, Eur. Phys. J. A **74**, 715 (1932).

[3] P. W. Anderson and J. M. Rowell, Probable Observation of the Josephson Superconducting Tunneling Effect, Phys. Rev. Lett. **10**, 230 (1963).

[4] B. D. Josephson, Possible new effects in superconductive tunnelling, Phys. Lett. **1**, 251 (1962).

[5] I. Žutić, J. Fabian, and S. Das Sarma, Spintronics: Fundamentals and applications, Rev. Mod. Phys. **76**, 323 (2004).

[6] S. Bandyopadhyay and M. Cahay, Reexamination of some spintronic field-effect device concepts, Appl. Phys. Lett. **85**, 1433 (2004).

[7] W. J. M. Naber, S. Faez, and W. G. van der Wiel, Organic spintronics, J. Phys. D: Appl. Phys. **40**, R205 (2007).

[8] S. Bandyopadhyay and M. Cahay, *Introduction to Spintronics* (CRC Press, Boca Raton, 2016).

[9] G. Dresselhaus, Spin-orbit coupling effects in zinc blende structures, Phys. Rev. **100**, 580 (1955).

[10] E. I. Rashba, Properties of semiconductors with an extremum loop. 1. Cyclotron and combinational resonance in a magnetic field perpendicular to the plane of the loop, Sov. Phys. Solid State **2**, 1109 (1960).

[11] Yu. A. Bychkov and E. I. Rashba, Properties of a 2D electron gas with lifted spectral degeneracy, JEPT Lett. **39**, 78 (1984).

[12] A. Bansil, H. Lin, and T. Das, Colloquium: Topological band theory, Rev. Mod. Phys. **88**, 021004 (2016).

[13] T. Jungwirth, J. Wunderlich, and K. Olejnik, Spin Hall effect devices, Nat. Mater. **11**, 382 (2012).

[14] A. Manchon, H. C. Koo, J. Nitta, S. M. Frolov, and R. A. Duine, New perspectives for Rashba spin-orbit coupling, Nat. Mater. **14**, 871 (2015).

[15] V. K. Joshi, Spintronics: A contemporary review of emerging electronics devices, Eng. Sci. Technol. Int. J. **19**, 1503 (2016).

[16] A. Soumyanarayanan, N. Reyren, A. Fert, and Ch. Panagopoulos, Emergent phenomena induced by spin-orbit coupling at surfaces and interfaces, Nature (London) **539**, 509 (2016).

[17] C. Chappert, A. Fert, and F. N. Van Dau, The emergence of spin electronics in data storage, Nat. Mater. **6**, 813 (2007).

[18] E. Knill, Quantum computing with realistically noisy devices, Nature (London) **434**, 39 (2005).

[19] J. S. Friedman, E. R. Fadel, B. W. Wessels, D. Querlioz, and A. V. Sahakian, Bilayer avalanche spin-diode logic, AIP Adv. **5**, 117102 (2015).

[20] Y. Wang, A. Kumar, T.-Y. Wu, and D. S. Weiss, Single-qubit gates based on targeted phase shifts in a 3D neutral atom array, Science **352**, 1562 (2016).

[21] J. Linder and J. W. A. Robinson, Superconducting spintronics, Nat. Phys. **11**, 307 (2015).

[22] E. C. Gingrich, B. M. Niedzielski, J. A. Glick, Y. Wang, D. L. Miller, R. Loloee, W. P. Pratt, Jr., and N. O. Birge, Controllable 0-π Josephson junctions containing a ferromagnetic spin valve, Nat. Phys. **12**, 564 (2016).

[23] A. Costa, P. Högl, and J. Fabian, Magnetoanisotropic Josephson effect due to interfacial spin-orbit fields in superconductor/ferromagnet/superconductor junctions, Phys. Rev. B **95**, 024514 (2017).

[24] Z.-P. Niu, A spin triplet supercurrent in half metal ferromagnet/superconductor junctions with the interfacial Rashba spin-orbit coupling, Appl. Phys. Lett. **101**, 062601 (2012).

[25] J. Alicea, New directions in the pursuit of Majorana fermions in solid state systems, Rep. Prog. Phys. **75**, 076501 (2012).

[26] C. W. J. Beenakker, Search for Majorana fermions in superconductors, Annu. Rev. Condens. Matter Phys. **4**, 113 (2013).

[27] S. R. Elliott and M. Franz, Colloquium: Majorana fermions in nuclear, particle, and solid-state physics, Rev. Mod. Phys. **87**, 137 (2015).

[28] A. Y. Kitaev, Unpaired Majorana fermions in quantum wires, Phys. Usp. **44**, 131 (2001).

[29] V. Mourik, K. Zuo, S. M. Frolov, S. R. Plissard, E. P. A. M. Bakkers, and L. P. Kouwenhoven, Signatures of Majorana Fermions in hybrid superconductor-semiconductor nanowire devices, Science **336**, 1003 (2012).

[30] A. Das, Y. Ronen, Y. Most, Y. Oreg, M. Heiblum, and H. Shtrikman, Zero-bias peaks and splitting in an Al-InAs nanowire topological superconductor as a signature of Majorana fermions, Nat. Phys. **8**, 887 (2012).

[31] M. T. Deng, C. L. Yu, G. Y. Huang, M. Larsson, P. Caroff, and H. Q. Xu, Anomalous zero-bias conductance peak in a Nb-InSb nanowire-Nb hybrid device, Nano Lett. **12**, 6414 (2012).

[32] H. O. H. Churchill, V. Fatemi, K. Grove-Rasmussen, M. T. Deng, P. Caroff, H. Q. Xu, and C. M. Marcus, Superconductor-nanowire devices from tunneling to the multichannel regime: Zero-bias oscillations and magnetoconductance crossover, Phys. Rev. B **87**, 241401 (2013).

[33] B. E. Feldman, M. T. Randeria, J. Li, S. Jeon, Y. Xie, Z. Wang, I. K. Drozdov, B. Andrei, and A. Yazdani, High-resolution studies of the Majorana atomic chain platform, Nat. Phys. **13**, 286 (2017).

[34] M. T. Deng, S. Vaitiekenas, E. B. Hansen, J. Danon, M. Leijnse, K. Flensberg, J. Nygård, P. Krogstrup, and C. M. Marcus, Majorana bound state in a coupled quantum-dot hybrid-nanowire system, Science **354**, 1557 (2016).

[35] A. Ptok, A. Kobiałka, and T. Domański, Controlling the bound states in a quantum-dot hybrid nanowire, Phys. Rev. B **96**, 195430 (2017).

[36] L. Fu and C. L. Kane, Superconducting Proximity Effect and Majorana Fermions at the Surface of a Topological Insulator, Phys. Rev. Lett. **100**, 096407 (2008).

[37] S. Tewari, S. Das Sarma, Chetan Nayak, Ch. Zhang, and P. Zoller, Quantum Computation Using Vortices and Majorana Zero Modes of a $p_x + ip_y$ Superfluid of Fermionic Cold Atoms, Phys. Rev. Lett. **98**, 010506 (2007).

[38] F.-Ch. Hsu, J.-Y. Luo, K.-W. Yeh, T.-K. Chen, T.-W. Huang, P. M. Wu, Y.-Ch. Lee, Y.-L. Huang, Y.-Y. Chu, D.-Ch. Yan, and M.-K. Wu, Superconductivity in the PbO-type structure α-FeSe, Proc. Natl. Acad. Sci. USA **105**, 14262 (2008).

[39] W. Qing-Yan, L. Zhi, Z. Wen-Hao, Z. Zuo-Cheng, Z. Jin-Song, L. Wei, D. Hao, O. Yun-Bo, D. Peng, Ch. Kai, W. Jing, S. Can-Li, H. Ke, J. Jin-Feng, J. Shuai-Hua, W. Ya-Yu, W. Li-Li, Ch. Xi, M. Xu-Cun, and X. Qi-Kun, Interface-induced high-temperature superconductivity in single unit-cell FeSe films on $SrTiO_3$, Chin. Phys. Lett. **29**, 037402 (2012).

[40] D. Liu, W. Zhang, D. Mou, J. He, Y.-B. Ou, Q.-Y. Wang, Z. Li, L. Wang, L. Zhao, S. He, Y. Peng, X. Liu, Ch. Chen, L. Yu, G. Liu, X. Dong, J. Zhang, Ch. Chen, Z. Xu, J. Hu, X. Chen, X. Ma, Q. Xue, and X. J. Zhou, Electronic origin of high-temperature

superconductivity in single-layer FeSe superconductor, Nat. Commun. **3**, 931 (2012).

[41] S. He, J. He, W. Zhang, L. Zhao, D. Liu, X. Liu, D. Mou, Y.-B. Ou, Q.-Y. Wang, Z. Li, L. Wang, Y. Peng, Y. Liu, Ch. Chen, L. Yu, G. Liu, X. Dong, J. Zhang, Ch. Chen, Z. Xu, X. Chen, X. Ma, Q. Xue, and X. J. Zhou, Phase diagram and electronic indication of high-temperature superconductivity at 65 K in single-layer FeSe films, Nat. Mater. **12**, 605 (2013).

[42] S. Tan, Y. Zhang, M. Xia, Z. Ye, F. Chen, X. Xie, R. Peng, D. Xu, Q. Fan, H. Xu, J. Jiang, T. Zhang, X. Lai, T. Xiang, J. Hu, B. Xie, and D. Feng, Interface-induced superconductivity and strain-dependent spin density waves in FeSe/$SrTiO_3$ thin films, Nat. Mater. **12**, 634 (2013).

[43] G. Zhou, D. Zhang, Ch. Liu, Ch. Tang, X. Wang, Z. Li, C. Song, S. Ji, K. He, L. Wang, X. Ma, and Q.-K. Xue, Interface induced high temperature superconductivity in single unit-cell FeSe on $SrTiO_3$(110), Appl. Phys. Lett. **108**, 202603 (2016).

[44] P. Zhang, X.-L. Peng, T. Qian, P. Richard, X. Shi, J.-Z. Ma, B. B. Fu, Y.-L. Guo, Z. Q. Han, S. C. Wang, L. L. Wang, Q.-K. Xue, J. P. Hu, Y.-J. Sun, and H. Ding, Observation of high-T_c superconductivity in rectangular FeSe/$SrTiO_3$(110) monolayers, Phys. Rev. B **94**, 104510 (2016).

[45] X. Wu, X. Dai, Y. Liang, C. Le, H. Fan, and J. Hu, Density functional calculations of a staggered FeSe monolayer on a $SrTiO_3$ (110) surface, Phys. Rev. B **94**, 045114 (2016).

[46] Z. Zhong, A. Tóth, and K. Held, Theory of spin-orbit coupling at $LaAlO_3$/$SrTiO_3$ interfaces and $SrTiO_3$ surfaces, Phys. Rev. B **87**, 161102 (2013).

[47] N. R. Wilson, P. V. Nguyen, K. Seyler, P. Rivera, A. J. Marsden, Z. P. L. Laker, G. C. Constantinescu, V. Kandyba, A. Barinov, N. D. M. Hine, X. Xu, and D. H. Cobden, Determination of band offsets, hybridization, and exciton binding in 2D semiconductor heterostructures, Sci. Adv. **3**, e1601832 (2017).

[48] M. Q. He, J. Y. Shen, A. P. Petrović, Q. L. He, H. C. Liu, Y. Zheng, C. H. Wong, Q. H. Chen, J. N. Wang, K. T. Law, I. K. Sou, and R. Lortz, Pseudogap and proximity effect in the Bi_2Te_3/$Fe_{1+y}Te$ interfacial superconductor, Sci. Rep. **6**, 32508 (2016).

[49] A. Avsar, J. Y. Tan, T. Taychatanapat, J. Balakrishnan, G. K. W. Koon, Y. Yeo, J. Lahiri, A. Carvalho, A. S. Rodin, E. C. T. O'Farrell, G. Eda, A. H. Castro Neto, and B. Özyilmaz, Spin-orbit proximity effect in graphene, Nat. Commun. **5**, 4875 (2014).

[50] D. Marchenko, A. Varykhalov, M. R. Scholz, G. Bihlmayer, E. I. Rashba, A. Rybkin, A. M. Shikin, and O. Rader, Giant Rashba splitting in graphene due to hybridization with gold, Nat. Commun. **3**, 1232 (2012).

[51] Z. Qiao, W. Ren, H. Chen, L. Bellaiche, Z. Zhang, A. H. MacDonald, and Q. Niu, Quantum Anomalous Hall Effect in Graphene Proximity Coupled to an Antiferromagnetic Insulator, Phys. Rev. Lett. **112**, 116404 (2014).

[52] R. Beiranvand, H. Hamzehpour, and M. Alidoust, Nonlocal Andreev entanglements and triplet correlations in graphene with spin-orbit coupling, Phys. Rev. B **96**, 161403(R) (2017).

[53] R. Beiranvand, H. Hamzehpour, and M. Alidoust, Tunable anomalous Andreev reflection and triplet pairings in spin-orbit-coupled graphene, Phys. Rev. B **94**, 125415 (2016).

[54] Z. Wang, C. Tang, R. Sachs, Y. Barlas, and J. Shi, Proximity-Induced Ferromagnetism in Graphene Revealed by the Anomalous Hall Effect, Phys. Rev. Lett. **114**, 016603 (2015).

[55] J. B. S. Mendes, O. A. Santos, L. M. Meireles, R. G. Lacerda, L. H. Vilela-Leão, F. L. A. Machado, R. L. Rodríguez-Suárez, A. Azevedo, and S. M. Rezende, Spin-Current to Charge-Current Conversion and Magnetoresistance in a Hybrid Structure of Graphene and Yttrium Iron Garnet, Phys. Rev. Lett. **115**, 226601 (2015).

[56] S. Dushenko, H. Ago, K. Kawahara, T. Tsuda, S. Kuwabata, T. Takenobu, T. Shinjo, Y. Ando, and M. Shiraishi, Gate-Tunable Spin-Charge Conversion and the Role of Spin-Orbit Interaction in Graphene, Phys. Rev. Lett. **116**, 166102 (2016).

[57] P. Chudzinski, Spin-orbit coupling and proximity effects in metallic carbon nanotubes, Phys. Rev. B **92**, 115147 (2015).

[58] Y. Q. Zhang, N. Y. Sun, W. R. Che, X. L. Li, J. W. Zhang, R. Shan, Z. G. Zhu, and G. Su, Manipulating effective spin orbit coupling based on proximity effect in magnetic bilayers, Appl. Phys. Lett. **107**, 082404 (2015).

[59] J. Balakrishnan, G. Kok Wai Koon, M. Jaiswal, A. H. Castro Neto, and B. Ozyilmaz, Colossal enhancement of spin-orbit coupling in weakly hydrogenated graphene, Nat. Phys. **9**, 284 (2013).

[60] A. H. Castro Neto and F. Guinea, Impurity-Induced Spin-Orbit Coupling in Graphene, Phys. Rev. Lett. **103**, 026804 (2009).

[61] L. Fu, C. L. Kane, and E. J. Mele, Topological Insulators in Three Dimensions, Phys. Rev. Lett. **98**, 106803 (2007).

[62] X.-L. Qi and S.-Ch. Zhang, Topological insulators and superconductors, Rev. Mod. Phys. **83**, 1057 (2011).

[63] A. P. Mackenzie and Y. Maeno, The superconductivity of Sr_2RuO_4 and the physics of spin-triplet pairing, Rev. Mod. Phys. **75**, 657 (2003).

[64] F. S. Bergeret, A. F. Volkov, and K. B. Efetov, Odd triplet superconductivity and related phenomena in superconductor-ferromagnet structures, Rev. Mod. Phys. **77**, 1321 (2005).

[65] M. Sato and S. Fujimoto, Topological phases of noncentrosymmetric superconductors: Edge states, Majorana fermions, and non-Abelian statistics, Phys. Rev. B **79**, 094504 (2009).

[66] M. Smidman, M. B. Salamon, H. Q. Yuan, and D. F. Agterberg, Superconductivity and spin-orbit coupling in non-centrosymmetric materials: A review, Rep. Prog. Phys. **80**, 036501 (2017).

[67] M. Sato, Y. Takahashi, and S. Fujimoto, Non-Abelian topological orders and Majorana Fermions in spin-singlet superconductors, Phys. Rev. B **82**, 134521 (2010).

[68] L. P. Gor'kov and E. I. Rashba, Superconducting 2D System with Lifted Spin Degeneracy: Mixed Singlet-Triplet State, Phys. Rev. Lett. **87**, 037004 (2001).

[69] Ch. Zhang, S. Tewari, R. M. Lutchyn, and S. Das Sarma, $p_x + ip_y$ Superfluid from s-wave Interactions of Fermionic Cold Atoms, Phys. Rev. Lett. **101**, 160401 (2008).

[70] J. Alicea, Majorana fermions in a tunable semiconductor device, Phys. Rev. B **81**, 125318 (2010).

[71] K. Seo, L. Han, and C. A. R. Sá de Melo, Topological phase transitions in ultracold Fermi superfluids: The evolution from Bardeen-Cooper-Schrieffer to Bose-Einstein-condensate superfluids under artificial spin-orbit fields, Phys. Rev. A **85**, 033601 (2012).

[72] T. Yu and M. W. Wu, Gapped triplet p-wave superconductivity in strong spin-orbit-coupled semiconductor quantum wells in proximity to s-wave superconductor, Phys. Rev. B **93**, 195308 (2016).

[73] Y. Tanaka, T. Yokoyama, and N. Nagaosa, Manipulation of the Majorana Fermion, Andreev Reflection, and Josephson Current on Topological Insulators, Phys. Rev. Lett. **103**, 107002 (2009).
[74] M. Alidoust and K. Halterman, Long-range spin-triplet correlations and edge spin currents in diffusive spin-orbit coupled SNS hybrids, with a single spin-active interface, J. Phys: Cond. Matt. **27**, 235301 (2015).
[75] M. Alidoust and K. Halterman, Spontaneous edge accumulation of spin currents in finite-size two-dimensional diffusive spin-orbit coupled SFS heterostructures, New J. Phys. **17**, 033001 (2015).
[76] Z. Li, L. Covaci, M. Berciu, D. Baillie, and F. Marsiglio, Impact of spin-orbit coupling on the Holstein polaron, Phys. Rev. B **83**, 195104 (2011).
[77] Z. Li, L. Covaci, and F. Marsiglio, Impact of Dresselhaus versus Rashba spin-orbit coupling on the Holstein polaron, Phys. Rev. B **85**, 205112 (2012).
[78] A. Ptok and D. Crivelli, The Fulde-Ferrell-Larkin-Ovchinnikov state in pnictides, J. Low Temp. Phys. **172**, 226 (2013).
[79] C. J. Halboth and W. Metzner, *d*-wave Superconductivity and Pomeranchuk Instability in the Two-Dimensional Hubbard Model, Phys. Rev. Lett. **85**, 5162 (2000).
[80] A. Ptok, D. Crivelli, and K. J. Kapcia, Change of the sign of superconducting intraband order parameters induced by interband pair hopping interaction in iron-based high-temperature superconductors, Supercond. Sci. Technol. **28**, 045010 (2015).
[81] A. Ptok, Influence of $s_{\pm}$ symmetry on unconventional superconductivity in pnictides above the Pauli limit—two-band model study, Eur. Phys. J. B **87**, 2 (2014).
[82] R. Micnas, J. Ranninger, and S. Robaszkiewicz, Superconductivity in narrow-band systems with local nonretarded attractive interactions, Rev. Mod. Phys. **62**, 113 (1990).
[83] J. Bardeen, L. N. Cooper, and J. R. Schrieffer, Microscopic theory of superconductivity, Phys. Rev. **106**, 162 (1957).
[84] J. Bardeen, L. N. Cooper, and J. R. Schrieffer, Theory of superconductivity, Phys. Rev. **108**, 1175 (1957).
[85] A. Ptok and D. Crivelli, Influence of finite size effects on the Fulde-Ferrell-Larkin-Ovchinnikov state, Commun. Comput. Phys. **21**, 748 (2017).
[86] M. Januszewski, A. Ptok, D. Crivelli, and B. Gardas, GPU-based acceleration of free energy calculations in solid state physics, Comput. Phys. Commun. **192**, 220 (2015).
[87] M. Maśka, Self-energy approach to the t-J model, Phys. Rev. B **48**, 1160 (1993).
[88] G. Chen, M. Gong, and Ch. Zhang, BCS-BEC crossover in spin-orbit-coupled two-dimensional Fermi gases, Phys. Rev. A **85**, 013601 (2012).
[89] H. Shi, P. Rosenberg, S. Chiesa, and S. Zhang, Rashba Spin-Orbit Coupling, Strong Interactions, and the BCS-BEC Crossover in the Ground State of the Two-Dimensional Fermi Gas, Phys. Rev. Lett. **117**, 040401 (2016).
[90] J. Lee and D.-H. Kim, Induced interactions in the BCS-BEC crossover of two-dimensional Fermi gases with Rashba spin-orbit coupling, Phys. Rev. A **95**, 033609 (2017).
[91] N. R. Werthamer, E. Helfand, and P. C. Hohenberg, Temperature and purity dependence of the superconducting critical field, H_{c2}. III. Electron spin and spin-orbit effects, Phys. Rev. **147**, 295 (1966).
[92] H. Lei, R. Hu, E. S. Choi, J. B. Warren, and C. Petrovic, Pauli-limited upper critical field of $Fe_{1+y}Te_{1-x}Se_x$, Phys. Rev. B **81**, 094518 (2010).
[93] F. Wolff-Fabris, H. Lei, J. Wosnitza, and C. Petrovic, Evolution of the Pauli spin-paramagnetic effect on the upper critical fields of single-crystalline $K_xFe_{2-y}Se_{2-z}S_z$, Phys. Rev. B **90**, 024505 (2014).
[94] K.-Ch. Weng and C. D. Hu, The *p*-wave superconductivity in the presence of Rashba interaction in 2DEG, Sci. Rep. **6**, 29919 (2016).
[95] I. Bloch, J. Dalibard, and W. Zwerger, Many-body physics with ultracold gases, Rev. Mod. Phys. **80**, 885 (2008).
[96] L. Jiang, X.-J. Liu, H. Hu, and H. Pu, Rashba spin-orbit-coupled atomic Fermi gases, Phys. Rev. A **84**, 063618 (2011).
[97] V. Galitski and I. B. Spielman, Spin-orbit coupling in quantum gases, Nature (London) **494**, 49 (2013).
[98] Z. Fu, L. Huang, Z. Meng, P. Wang, L. Zhang, S. Zhang, H. Zhai, P. Zhang, and J. Zhang, Production of Feshbach molecules induced by spin-orbit coupling in Fermi gases, Nat. Phys. **10**, 110 (2014).
[99] F. Grusdt, T. Li, I. Bloch, and E. Demler, Tunable spin-orbit coupling for ultracold atoms in two-dimensional optical lattices, Phys. Rev. A **95**, 063617 (2017).
[100] J. Linder and A. Sudbø, Theory of Andreev reflection in junctions with iron-based high-T_c superconductors, Phys. Rev. B **79**, 020501 (2009).